


Unacylated Ghrelin Enhances Satellite Cell Function and Relieves the Dystrophic Phenotype in Duchenne Muscular Dystrophy mdx Model

SIMONE REANO,^{a*} ELIA ANGELINO,^{a*} MICHELE FERRARA,^a VALERIA MALACARNE,^a HANA SUSTOVA,^a OMAR SABRY,^a EMANUELA AGOSTI,^a SARA CLERICI,^a GIULIA RUOZI,^b LORENA ZENTILIN,^b FLAVIA PRODAM,^c STEFANO GEUNA,^d MAURO GIACCA,^b ANDREA GRAZIANI,^{a*} NICOLETTA FILIGHEDDU ^{a*}

^aDepartment of Translational Medicine, University of Piemonte Orientale, Novara, Italy and Istituto Interuniversitario di Miologia (IIM); ^dDepartment of Clinical and Biological Sciences, University of Torino and Neuroscience Institute Cavalieri Ottolenghi (NICO), Orbassano (TO), Italy; ^bInternational Centre for Genetic Engineering and Biotechnology (ICGEB), Trieste, Italy; ^cDepartment of Health Sciences, University of Piemonte Orientale, Novara, Italy

*Contributed equally.

Correspondence: Nicoletta Filigheddu, Ph.D., Department of Translational Medicine, University of Piemonte Orientale, Via Solaroli 17, 28100 Novara, Italy. Telephone: +39-0321-660-529; e-mail: nicoletta.filigheddu@med.uniupo.it; or Andrea Graziani, Ph.D., Università Vita-Salute San Raffaele, via Olgettina 58, 20132, Milano, Italy. Telephone: +39-02-2643-3823; e-mail: graziani.andrea@hsr.it

Received August 10, 2016; accepted for publication April 6, 2017; first published online in *STEM CELLS EXPRESS* April 24, 2017.

© AlphaMed Press
1066-5099/2017/\$30.00/0

<http://dx.doi.org/10.1002/stem.2632>

Key Words. Satellite cell self-renewal • Skeletal muscle regeneration • Ghrelin • Duchenne muscular dystrophy • mdx dystrophic mice

ABSTRACT

Muscle regeneration depends on satellite cells (SCs), quiescent precursors that, in consequence of injury or in pathological states such as muscular dystrophies, activate, proliferate, and differentiate to repair the damaged tissue. A subset of SCs undergoes self-renewal, thus preserving the SC pool and its regenerative potential. Unacylated ghrelin (UnAG) is a circulating hormone that protects muscle from atrophy, promotes myoblast differentiation, and enhances ischemia-induced muscle regeneration. Here we show that UnAG increases SC activity and stimulates Par polarity complex/p38-mediated asymmetric division, fostering both SC self-renewal and myoblast differentiation. Because of those activities on different steps of muscle regeneration, we hypothesized a beneficial effect of UnAG in mdx dystrophic mice, in which the absence of dystrophin leads to chronic muscle degeneration, defective muscle regeneration, fibrosis, and, at later stages of the pathology, SC pool exhaustion. Upregulation of UnAG levels in mdx mice reduces muscle degeneration, improves muscle function, and increases dystrophin-null SC self-renewal, maintaining the SC pool. Our results suggest that UnAG has significant therapeutic potential for preserving the muscles in dystrophies. *STEM CELLS* 2017;35:1733–1746

SIGNIFICANCE STATEMENT

Muscle dystrophies (MDs) are pathologies characterized by chronic degeneration of muscles. This induces a sustained and continuous regeneration that depends on satellite cells (SCs). Defective regeneration and SC pool exhaustion ultimately lead to the replacement of muscles with scar tissue and loss of functionality. Unacylated ghrelin (UnAG) is a circulating hormone with protective activities on skeletal muscles. Here we demonstrated that UnAG helps to maintain the pool of SCs and that it has a beneficial effect on muscles of dystrophic mice. UnAG could represent a novel treatment for MDs, either alone or as an adjuvant therapy for one of the promising stem cell-based therapies.

INTRODUCTION

Injuries or pathological states such as muscular dystrophies trigger regeneration in the adult skeletal muscle. Muscle regeneration is mainly sustained by a heterogeneous population of quiescent resident precursors, called satellite cells (SCs), characterized by the expression of the transcriptional factor Pax7 [1]. In consequence of injury, SCs activate, proliferate, and eventually differentiate to repair the damaged tissue and restore muscle function. A portion of SCs undergoes self-renewal through asymmetric division, thus maintaining the quiescent SC pool and allowing the muscle to retain its

regenerative potential [2, 3]. The asymmetric division generates two daughter cells with divergent fates: one proliferating myoblast expressing the marker of myogenic commitment MyoD (MyoD+) and one MyoD– quiescent SC preserving stem features. The differential expression of MyoD depends on the asymmetric segregation of the Par polarity complex during SC activation that leads to a polarized activation of p38 MAPK pathway, triggering MyoD expression in only one daughter cell [4, 5].

Ghrelin and unacylated ghrelin (UnAG) are circulating peptide hormones mainly produced by the stomach. Ghrelin derives from the

octanoylation of the prehormone by the ghrelin-O-acyltransferase (GOAT) enzyme [6, 7]. Acylation is required for the binding to the growth hormone secretagogue receptor-1a (GHSR-1a) to induce growth hormone release and to perform multiple endocrine functions [8, 9]. UnAG, the main circulating form of the peptide, does not bind to GHSR-1a but features several biological activities, including the enhancement of skeletal muscle regeneration induced by hindlimb ischemia [10, 11] and improvement of insulin sensitivity in skeletal muscle [12, 13]. Besides, UnAG shares with ghrelin numerous biological effects, among which the protection of skeletal muscle from atrophy [14, 15] and the promotion of myoblast differentiation [16].

While the mechanisms through which UnAG protects skeletal muscle from atrophy and insulin resistance have been described [12–14], the cellular and molecular mechanisms mediating UnAG ability to enhance muscle regeneration remain to be elucidated. Here we show that UnAG affects multiple stages of muscle regeneration, including SC activation, proliferation, and self-renewal, the latter through induction of SC asymmetric division mediated by PKC λ /i-Par6 complex formation and asymmetric activation of p38. Moreover, UnAG induces the differentiation of committed myoblasts, thus promoting the regeneration of injured muscles. Based on UnAG ability to enhance skeletal muscle regeneration, we hypothesized that UnAG could have a therapeutic importance for muscle dystrophies. Duchenne muscular dystrophy (DMD) is characterized by the absence of the dystrophin protein, whose main function is to connect the myofiber cytoskeleton to the extracellular matrix through the dystrophin-associated glycoprotein complex. In the absence of dystrophin, myofibers are extremely susceptible to contraction-induced damage, with the consequent chronic degeneration [17]. Moreover, dystrophin-null SCs display an impairment of self-renewal and asymmetric division that results in a faulty myogenic progression and, thus, in a defective regenerative process [18, 19]. We show that upregulation of circulating or local UnAG levels in mdx mice improves the dystrophic phenotype, including muscle architecture and functionality. Moreover, UnAG blunts the self-renewal defect of dystrophin-null SCs, thus preserving the SC pool at later stages of the pathology.

MATERIALS AND METHODS

Animals

Animal experiments were performed according to procedures approved by the Institutional Animal Care and Use Committee at the University of Piemonte Orientale. Male mice, matched for age and weight, were used for all experiments. Dystrophin-deficient mdx mice (C57BL/10ScSn-Dmdmdx/J) and C57BL/6-Tg(CAG-EGFP)131Osb/LeySopJ mice with ubiquitous GFP expression were from The Jackson Laboratory (Bar Harbor, ME, <https://www.jax.org/>); FVB1-Myh6/Ghrl and C57BL/6-Myh6/Ghrl transgenic mice were generated as previously described [14]. Animals were fed ad libitum and had unrestricted access to drinking water. The light/dark cycle in the room consisted of 12/12 hours with artificial light. To generate dystrophic mice overexpressing the ghrelin gene, C57BL/6J hemizygous Myh6/Ghrl male mice were bred to homozygous Dmd^{mdx/mdx} female mice to yield an equal proportion of male mdx^{Tg+} and mdx^{Tg-}

littermate controls. mdx mice bearing Myh6/Ghrl transgene were identified by PCR genotyping. High levels of plasmatic UnAG in mdx^{Tg+} were confirmed by EIA kit (SPIbio Bertin Pharma, Montigny le Bretonneux, France, <http://www.bertin-pharma.com/>) according to the manufacturer's instructions. The numbers of mice estimated sufficient to detect a difference between two means as large as 1 SD unit with 80% power and a significance level of 95% at Student's *t* test were calculated with the program by R.V. Lenth (www.stat.uiowa.edu/~rlenth/Power/index.html). The investigators conducting the experiments were blind to the experimental group assessed. The investigators quantifying the experimental outcomes were maintained blinded to the animal group or intervention. Finally, the statistic evaluation of the experimental data was performed by another investigator not directly involved in data collection and parameter measurement.

Reagents

Rat UnAG peptide was purchased from PolyPeptide Laboratories (Strasbourg, France, <http://www.polypeptide.com/>). Media and fetal bovine serum (FBS) were from Gibco (Thermo Fisher Scientific, Ashford, UK, <https://www.thermofisher.com/>), horse serum (HS) from PAA (GE Healthcare, Little Chalfont, UK, <http://www3.gehealthcare.com/>), and media supplements, unless otherwise specified, were from Sigma-Aldrich (Paisley, UK, <http://www.sigmaaldrich.com>).

Cardiotoxin-Induced Muscle Regeneration

Experiments on muscle regeneration were conducted on adult male FVB1 and FVB1-Myh6/Ghrl mice matched for age and weight. Cardiotoxin (CTX) from *Naja mossaibica mossaibica* (Latoxan, Portes-lès-Valence, France, <http://www.latoxan.net/>) was dissolved in sterile saline to a final concentration of 10 μ M. Mice were anesthetized by isoflurane inhalation and hindlimbs were shaved and cleaned with alcohol. Tibialis anterior (TA) muscles were injected with 45 μ l of CTX with a 30-gauge needle, with 15 microinjections of 3 μ l CTX each in the mid-belly of the muscle to induce a homogeneous damage. The TA muscles of the contralateral hindlimbs were injected with saline. After injection, animals were kept under a warming lamp until recovery.

For some experiments, immediately after CTX administration, a single intraperitoneal injection of 5-bromo-2'-deoxyuridine (BrdU) (6 μ g/g mouse) was given, followed by BrdU administered ad libitum in drinking water (2.5 mg/ml) for 7 days.

Histological Analysis

Muscles were trimmed of tendons and adhering nonmuscle tissue, mounted in Killik embedding medium (Bio-optica, Milan, Italy, <http://www.bio-optica.it/>), frozen in liquid-nitrogen-cooled isopentane, and stored at -80°C . Transverse muscle sections (7 μ m) were cryosectioned from the mid-belly of each muscle. Sections were stained with hematoxylin/eosin to reveal general muscle architecture. Images of whole muscle sections were acquired with the slide scanner Pannoramic Midi 1.14 (3D Histech, Budapest, Hungary, <http://www.3dhitech.com/>) and cross-sectional areas (CSA) of centronucleated fibers quantified with ImageJ software (v1.49o). Muscle collagen content was assessed with Masson trichromic staining.

To quantify muscle damage and areas of focal necrosis, 1% wt/vol Evans blue dye (EBD) was injected intraperitoneally (5 μ l/g of animal weight). Muscles were collected 20 hours after EBD injection. Sections 7- μ m thick were cryosectioned, and EBD uptake was detected as red epifluorescence and quantified as above.

SC Isolation and Culture

Primary myoblasts were isolated from the main hindlimb muscles (TA, gastrocnemius, quadriceps [QUAD], extensor digitorum longus [EDL], soleus) and diaphragm. Muscles were cut with a lancet into small fragments (about 3 mm³) and further inspected to eliminate, as much as possible, any remaining connective tissue. The mass was resuspended in 3 ml of 0.1% pronase and incubated for 1 hour at 37°C for digestion. The suspension was then centrifuged at 400g for 5 minutes and the pellet resuspended in DMEM 10% HS medium, passed several times through a serological pipette, filtered through 40 μ m strainers, and further centrifuged at 400g for 10 minutes. SCs were separated from fibroblasts and other cells using the SC Isolation Kit (MACS Miltenyi Biotec, Milan, Italy) following the manufacturer's instructions. After isolation, SCs were either plated on gelatin-coated dishes or immediately used in muscle transplantation experiments.

Plated cells were cultured in growth medium (GM), Dulbecco's Modified Eagle's Medium (DMEM) with 20% FBS, 10% HS, 1% chicken embryo extract (CEE, USBiological Life Sciences, Salem, MA, <https://www.usbio.net/>), and 10 ng/ml FGF-2 (Peprotech Inc., London, U.K., <http://www.peprotech.com>). When cells reached 70%–80% of confluence, GM was shifted into differentiation medium (DM), DMEM with 5% HS for 3 days. UnAG (100 nM) was added simultaneously to DM.

SC Transplantation

To facilitate cell engraftment, one day before muscle transplantation, CTX injection was performed in the mid-belly of TA muscles of recipient mice. SCs were isolated from C57BL/6-Tg(CAG-EGFP)1310sb/LeySopJ (green fluorescence protein, GFP) mice and 100,000 cells, resuspended in serum-free DMEM, were injected in the previously injured recipient muscles. Contralateral TA muscles were injected with cell-free DMEM. Muscles were harvested 30 days after injection, fixed in 4% paraformaldehyde (PFA), and analyzed.

Myofiber Isolation and Culture

EDL muscles were digested in 0.2% collagenase type-I in DMEM for 60–70 minutes at 37°C. Muscles were mechanically dissociated, and single fibers liberated. After extensive washing, myofibers were either immediately fixed or cultured in low proliferation medium (LPM, DMEM supplemented with 10% HS and 0.5% CEE) in suspension. UnAG was added in LPM immediately after fiber seeding. At different time points after plating (6–72–96 hours) fibers were fixed in 4% PFA for 10 minutes.

For experiments with the chemotherapeutic drug AraC (Cytosine β -D-arabinofuranoside), myofibers were cultured for 72 hours in F12 medium supplemented with 15% HS and 1 nM FGF-2 in the presence or absence of 100 nM UnAG and then incubated with or without 100 μ M AraC for 48 hours and fixed (day 5).

Immunofluorescence

For Pax7 and BrdU detection, tissue sections were fixed in 4% PFA for 20 minutes, washed, permeabilized with cold methanol for 6 minutes, and then antigen-retrieved with sodium citrate (10 mM, 0.05% Tween in PBS) at 95°C for 30 minutes. For blocking the unspecific binding sites, slices were incubated in 4% bovine serum albumin (BSA) for 2 hours at RT and then with M.O.M. blocking reagent (Vector Laboratories, Burlingame, CA, <https://vectorlabs.com/>) for 1 hour at RT. Sections were stained with an anti-Pax7 antibody (1:100; Developmental Studies Hybridoma Bank, Iowa City, IA, <http://dshb.biology.uiowa.edu/>) and with anti-BrdU antibody (1:300; Bio-Rad, Segrate, MI, Italy, <http://www.bio-rad.com/>) overnight at 4°C. After washing, sections were incubated with the appropriate Alexa Fluor Dyes-conjugated secondary antibody (488-anti-mouse/anti-rabbit or 568-anti-rabbit; Thermo Fisher Scientific) for 1 hour at RT. 4',6-diamidino-2-phenylindole (DAPI) was incubated for 5 minutes.

For immunofluorescence with anti-laminin (1:200; Dako, Agilent Technologies, Santa Clara, CA, <http://www.agilent.com/>), anti-GFP (1:200; Thermo Fisher Scientific), and anti-embryonic MyHC (1:20; Developmental Studies Hybridoma Bank), after fixing, slices were permeabilized with 0.2% triton in 1% BSA for 15 minutes and blocked with 4% BSA for 30 minutes. One hour of incubation with primary antibodies was followed by 45 minutes of secondary antibody incubation at RT.

Images were acquired using the slide scanner Panoramic Midi Scanner 1.14 (3D Histech) and quantified with Panoramic viewer software or ImageJ v1.49o software. For immunofluorescence on isolated fibers and on cultured SCs, samples were fixed in 4% PFA for 10 minutes, permeabilized with 0.5% triton for 6 minutes and blocked with 4% BSA for 30 minutes. Primary antibodies to detect Pax7, MyoD (1:500; Santa Cruz Biotechnology, Dallas, TX, <https://www.scbt.com/>), myogenin (1:100; Developmental Studies Hybridoma Bank), and MyHC (1:100; Developmental Studies Hybridoma Bank) were incubated overnight at 4°C, and the secondary antibodies for 45 minutes at RT, followed by 5 minutes of DAPI. Images were acquired with a Leica CTR5500 B fluorescent microscope (Leica Biosystems, Wetzlar, Germany, <http://www.leicabiosystems.com/>) with the Leica Application SuiteX 1.5 software, and quantification was performed with ImageJ.

To evaluate the asymmetric division events of SC pairs, MyoD levels in each cell were obtained by subtracting the background from the nuclear fluorescence intensity (determined by overlap with DAPI staining). Cell pairs were scored "asymmetric" when the MyoD nuclear intensity of one daughter cell was $\leq 1\%$ ("MyoD-") and the other one was $> 1\%$ ("MyoD+") of the maximal intensity.

Asymmetric distribution of active p38 and PKC λ /i was evaluated by SC incubation with rabbit or mouse anti-phospho-p38^{T180/Y182} (1:200, Cell Signaling Technology, Beverly, MA, <https://www.cellsignal.com/>), rabbit anti-p38 (1:200, Cell Signaling Technology), rat anti-CD34 (1:200, BD Biosciences, Cowley, UK, <http://www.bdbiosciences.com/>), rabbit anti-PKC λ /i (1:200, Santa Cruz Biotechnology), rabbit anti-syndecan 4 (1:200, BioVision, Milpitas, CA, <http://www.biovision.com/>), and mouse anti-Pax7 (1:100; Developmental Studies Hybridoma Bank) followed by the appropriate Alexa Fluor Dyes-conjugated secondary antibodies (546 or 647 anti-mouse, 488 anti-rabbit, and 546

anti-rat; Thermo Fisher Scientific). Nuclei were counterstained with TO-PRO-3 iodide (1:100 Thermo Fisher Scientific). Images were acquired with Leica confocal microscope TCS SP2 using a 63X objective, NA = 1.32, equipped with LCS Leica confocal software. Asymmetry of phospho-p38^{T180/Y182} and PKC λ /i was quantified with ImageJ.

For the proximity ligation assay (PLA; Duolink from Sigma-Aldrich), myofiber-associated SCs were incubated with mouse anti-PKC λ /i (1:200, BD Bioscience) and rabbit anti-PAR3 (1:200, Merck Millipore) then processed according to the manufacturer's instructions.

Gene Expression Analysis

Total RNA from muscles was extracted by RNAzol. RNA was retro-transcribed with High-Capacity cDNA Reverse Transcription Kit (Thermo Fisher Scientific), and real-time PCR was performed with the StepOnePlus Real-Time PCR System (Thermo Fisher Scientific) using Mm00445450_m1 (*Ghrl*) and Mm00506384_m1 (*Ppif*) TaqMan assays.

Hanging Test

A wire-hanging test was used to assess whole-body muscle strength and endurance. The test was performed as previously described [20]. Briefly, mice were subjected to an 180 seconds-hanging test, during which "falling" and "reaching" scores were recorded. When a mouse fell or reached one of the sides of the wire, the falling score or reaching score was diminished or increased by 1, respectively. A Kaplan-Meier-like curve was created afterward. Moreover, the longest time between two falls was taken as the latency-to-fall value [21].

Statistical Analysis

All data were expressed as mean \pm SEM, absolute values, or percentages. For continuous variables, the variation between groups was compared by means of nonparametric Wilcoxon and Mann-Whitney *U* tests, as appropriate. When analyzing experiments acquired with different instruments, analysis of covariance (ANCOVA) was used to determine differences between groups by using the instrument as a covariate. Multiple logistic regression was used for trends. Statistical significance was assumed for $p < .05$. The statistical analysis was performed with SPSS for Windows version 17.0 (SPSS Inc; Chicago, IL).

RESULTS

UnAG Upregulation in *Myh6/Ghrl* Transgenic Mice Enhances Muscle Regeneration

Muscle damage induces the release, within the muscle, of several factors that activate SCs, triggering the expression of myogenic genes, such as *Myf5* and *MyoD* [22, 23] that eventually lead to the terminal differentiation of muscle precursors and their fusion among themselves or to the existing fibers. Muscle damage also induces, within the muscle, the expression of the ghrelin gene (Supporting Information Fig. 1) and the preproghrelin protein [24], suggesting that its products—ghrelin, UnAG, and obestatin—may participate in the repair process. Accordingly, exogenously administered obestatin and UnAG enhance muscle regeneration in CTX-injured gastrocnemii and in hindlimb ischemia, respectively [10, 11, 24].

Consistently, high levels of circulating UnAG in *Myh6/Ghrl* transgenic mice (Tg) [14] improved muscle regeneration of TA muscle after CTX injury (Fig. 1A–1C).

Despite no differences were noticeable between WT and Tg in noninjured muscle CSA distribution (Supporting Information Fig. 2A), at day 7 post CTX injury improved muscle regeneration in Tg mice was evidenced by a shift toward bigger areas of regenerating (i.e., centronucleated) fibers (Fig. 1B). This regeneration was accompanied by an increment in the number of regenerating fibers with ≥ 2 nuclei (Fig. 1C), suggesting an increase in myoblast differentiation and fusion during regeneration, in agreement with the pro-differentiative activity of UnAG in C2C12 myoblasts [16]. The shift toward bigger areas and the increased myoblast fusion did not translate into a hypertrophic phenotype, as at 15 days post-injury fiber distributions of WT and Tg overlapped (Supporting Information Fig. 2B). Consistently with the hypothesis that UnAG induces faster recovery, injured Tg muscles displayed more embryonal MyHC (eMyHC)-positive myofibers at day 3 post-CTX, although at day 7 no significant differences were observed in the number of eMyHC-expressing fibers (Supporting Information Fig. 2C–2E). Also, transient collagen deposition during regeneration tended to disappear more rapidly in Tg muscles between days 7 to 15 post-injury (Supporting Information Fig. 2F, 2G).

Though Tg mice do not overtly differ from their WT littermates [14], a closer examination of their not-injured muscles revealed a larger number of SCs, seen as Pax7+ nuclei, in both TA and QUAD from Tg animals (Fig. 1D, 1E). However, during the phase of intense proliferation following injury, SC number in muscles from Tg and WT were comparable (Supporting Information Fig. 2H–2I). This finding suggests that a UnAG-rich environment may confer a regenerative advantage, at least partially by promoting post-natal SC pool formation. In addition, transplant of SCs from GFP donor mice in muscles of Tg or WT recipient mice resulted, 30 days later, in $\sim 80\%$ increase in GFP+ fibers in Tg than in WT mice (Fig. 1F, 1G), suggesting that UnAG promotes skeletal muscle regeneration plausibly by acting on the transplanted SCs.

UnAG Promotes SC Activity and Their Asymmetric Division

To explore in detail the effects of UnAG on SCs, we isolated single fibers from WT muscles, thus maintaining SCs in an original niche-like environment [25], and we cultured them in the presence or absence of 100 nM UnAG. When cultured, SCs undergo activation and turn on MyoD expression (Pax7+/MyoD+). After 72 hours in culture, several clusters of myoblasts originated from a single SC are visible on myofibers. During this phase, the majority of activated SCs turns off Pax7 and commits to terminal differentiation (Pax7-/MyoD+), while a small subset undergoes self-renewal, retaining Pax7 but not MyoD expression (Pax7+/MyoD-) [26, 27]. UnAG treatment within 6 hours expanded the portion of activated SCs (Fig. 2A; Supporting Information Fig. 3A), within 72 hours it increased the number of cells in each cluster (Fig. 2B; Supporting Information Fig. 3B), and within 96 hours raised the portion of SCs that underwent self-renewal (Fig. 2C; Supporting Information Fig. 3C). Cotreatment with BrdU at the beginning of the experiment demonstrated that all cells underwent DNA replication, as the totality of Pax7+ cells within the

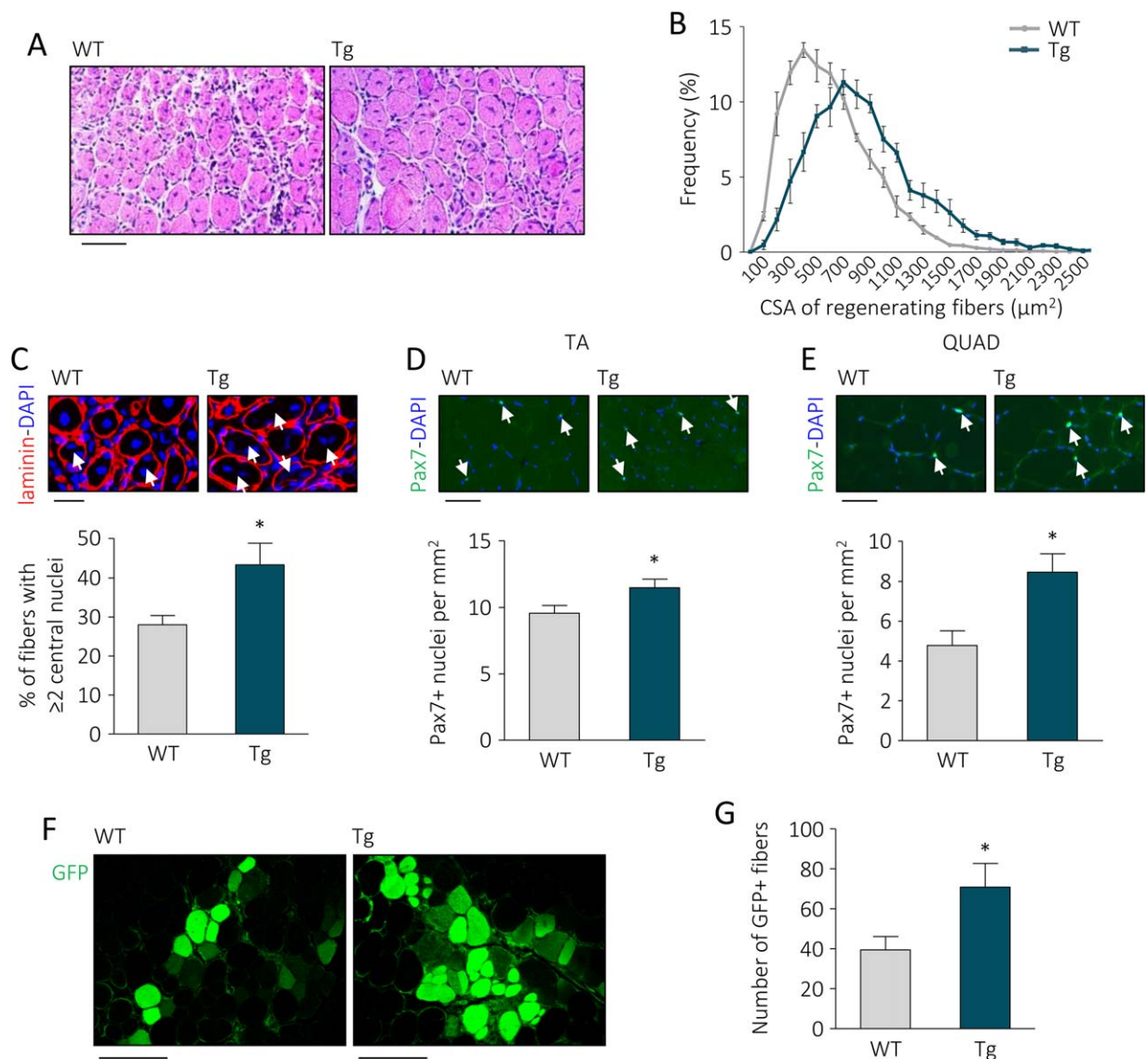


Figure 1. UnAG upregulation in *Myh6/Ghrl* transgenic mice enhances muscle regeneration, increases satellite cell (SC) number in non-injured muscles, and improves SC engraftment. **(A):** H&E representative images of WT and *Myh6/Ghrl* (Tg) TA muscle sections 7 days after cardiotoxin injury. Scale bar, 100 μm . **(B):** CSA frequency distribution of regenerating fibers in TA. Chi-square test was used to compare distributions. Trend $p < .01$. (CSA mean μm^2 : Tg 837.02 ± 55.41 ; WT 559.28 ± 15.81 ; $p < .05$). $N \geq 4$. **(C):** Representative images of laminin IF with DAPI staining of WT and Tg regenerating fibers and percentage of fibers with ≥ 2 central nuclei (arrows) over the total of regenerating fibers. Scale bar, 30 μm . Mean \pm SEM *, $p < .05$; $n \geq 4$. **(D, E):** Representative images and quantification of Pax7+ SCs/mm² (arrows) in noninjured TA (D) and QUAD (E) of WT and Tg mice. Mean \pm SEM Scale bars, 30 μm . *, $p < .05$; TA $n = 10$; QUAD $n = 5$. **(F, G):** Representative images (F) and quantification (G) of GFP+ myofibers in transplanted TA of WT and Tg mice. Scale bar, 200 μm . Mean \pm SEM *, $p < .05$; $n = 11$ (WT) and 12 (Tg). Abbreviations: CSA, cross-sectional areas; DAPI, 4',6-diamidino-2-phenylindole; GFP, green fluorescent protein; QUAD, quadriceps; TA, tibialis anterior; Tg, transgenic mice; WT, wild type mice.

clusters after 96 hours of UnAG treatment were also BrdU+ (Supporting Information Movies 1 and 2). Altogether, these data indicate that UnAG enhances SC activity by promoting their activation, expansion, and self-renewal.

SCs undergo self-renewal through asymmetric division that gives rise to a proliferating daughter cell and a quiescent daughter cell [4]. In culture, asymmetric division generally occurs during the first cellular division. This has been demonstrated by culturing myofibers with cytosine β -D-arabinofuranoside (AraC), a chemotherapeutic drug that selectively kills cycling cells and spares quiescent cells. Incubation of isolated myofibers with AraC during the first three days kills all myofiber-associated SCs, while the addition of AraC to the culture medium from day 3

to day 5 allows the detection of AraC-resistant Pax7+ SCs deriving from cells that divided at least once (Fig. 2D; [4, 28]). A higher number of Pax7+/MyoD- SCs was found in UnAG-treated myofibers after incubation with AraC from day 3 to 5 (Fig. 2E), suggesting that UnAG acts during SC first replications, likely regulating SC asymmetric division. Asymmetric division can be assessed by the quantification of myofiber-associated SC doublets, bona fide derived from a single SC after the first cell division, in which only one of the two daughter cells is MyoD+ [4]. UnAG treatment induced a sixfold increase in the percentage of SC doublets in which only one cell is MyoD+ (Fig. 2F, 2G), indicating that UnAG actually promotes SC asymmetric division. To verify whether UnAG induces self-renewal also in vivo,

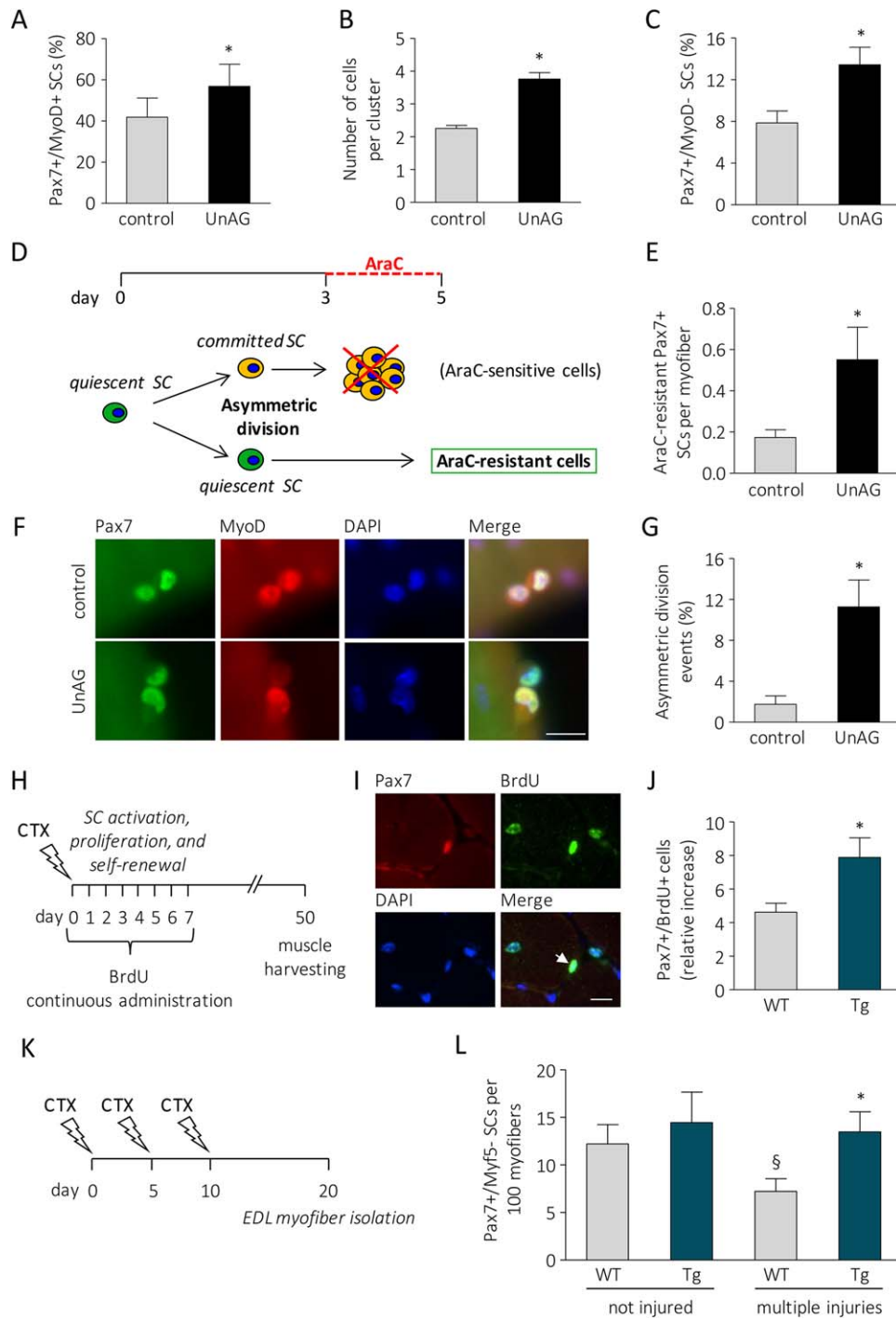


Figure 2. UnAG induces activation, proliferation, and self-renewal of SCs. **(A):** Percentage of MyoD+ SCs after 6 hours of treatment of isolated myofibers with 100 nM UnAG in low proliferation medium. ≥ 20 myofibers/treatment, ≥ 40 SCs/treatment. **(B):** Cells per cluster after 72 hours of treatment. ≥ 20 myofibers/treatment, ≥ 16 clusters/treatment, ≥ 2 SCs/cluster; $n = 3$ independent experiments. **(C):** Percentage of Pax7+/MyoD- SCs after 96 hours of treatment. Mean \pm SEM *, $p < .05$. ≥ 25 myofibers/treatment, ≥ 30 clusters/treatment, ≥ 3 SCs/cluster; $n = 3$ independent experiments. **(D):** Schematic of experiments with AraC to identify quiescent daughter SCs. **(E):** AraC-resistant Pax7+ cells. Mean \pm SEM *, $p < .05$; ≥ 25 myofibers/treatment, total araC-resistant Pax7+ SC $n = 13$ (control), 43 (UnAG); $n = 3$ independent experiments. **(F):** Representative images of SCs that underwent symmetric (control) or asymmetric (UnAG-treated) division. Scale bar, 20 μ m. **(G):** Percentage of asymmetric division events in SC doublets. Mean \pm SEM *, $p < .05$; for each experiment, ≥ 22 fibers/treatment; ≥ 22 doublets/treatment; $n = 3$ independent experiments. **(H):** Experimental design schematic: mice were daily treated with BrdU for the first 7 days after CTX injection. Muscles were harvested 50 days after injury. **(I):** Representative images of tibialis anterior transverse sections, arrow: Pax7+/BrdU+ nucleus. Scale bar, 40 μ m. **(J):** Pax7+/BrdU+ nuclei normalized to the contralateral SC number. Mean \pm SEM *, $p < .05$; $n \geq 8$. **(K):** SC forced exhaustion design schematic: 10 days after three injections of CTX at 5-days intervals, EDL fibers were isolated from injured hindlimbs and immediately fixed. **(L):** Number of Pax7+/Myf5- SCs in 100 isolated fibers. Mean \pm SEM *, $p < .05$ versus multiple injured WT; §, $p < .05$ versus not injured WT; $n \geq 8$. Abbreviations: AraC, cytosine β -D-arabinofuranoside; BrdU, 5-bromo-2'-deoxyuridine; CTX, cardiotoxin; DAPI, 4',6-diamidino-2-phenylindole; EDL, extensor digitorum longus; SC, satellite cell; UnAG, unacylated ghrelin.

we administered BrdU to WT and *Myh6/Ghrl* mice during the phase of intense myoblast proliferation post-injury (Fig. 2H). Since BrdU is incorporated in every cycling cell, when muscle regeneration is fully achieved, and SC proliferation no longer occurs, any cell positive for both BrdU and Pax7 (Fig. 2I) is a SC that cycled at least once and then underwent self-renewal [29]. Fifty days post-injury the number of Pax7⁺/BrdU⁺ SCs—normalized on SC number in the contralateral, noninjured muscle—was higher in *Myh6/Ghrl* than in WT muscles (Fig. 2J), demonstrating that upregulation of UnAG enhanced SC self-renewal also in vivo. SC self-renewal is of particular importance when skeletal muscle is subjected to repeated cycles of degeneration/regeneration that could lead to the progressive depletion of the SC pool; therefore, we assessed the impact of UnAG on the compartment of Myf5⁻ SCs, a subpopulation of SCs that undergoes depletion in an artificial model of SC pool exhaustion, obtained by multiple rounds of muscle injury (Fig. 2K, [30]). EDL fibers isolated from injured hindlimbs of WT mice displayed a 50% loss of Myf5⁻ SCs, while fibers from Tg mice maintained the number of Myf5⁻ SCs (Fig. 2L), demonstrating that UnAG helps to maintain the SC pool also upon repeated injuries.

UnAG Induces Satellite Cell Self-Renewal Through Par Complex Assembly and Activation of p38

UnAG exerts its anti-atrophic and pro-differentiative effects on skeletal muscle through activation of p38 [14, 16], a master regulator of SC activities, as its activation mediates either SC proliferation or differentiation [5, 31]. The role of p38 is particularly relevant in SC self-renewal, since the asymmetric segregation of phosphorylated p38 in dividing SCs regulates their asymmetric division, triggering MyoD protein expression in only one daughter cell [4, 5]. Treatment of myofibers with UnAG for 36 hours increased the asymmetric distribution of phosphorylated p38 in SCs without affecting total p38 uniform distribution (Fig. 3A, 3B; Supporting Information Fig. 4).

Since in the dividing SC phospho-p38 colocalizes with the atypical PKC λ /i [4], we assessed if UnAG could also enhance the asymmetric distribution of PKC λ /i. Indeed, UnAG treatment increased PKC λ /i localization in one of the two SC halves (Fig. 3C, 3D). Moreover, UnAG enhanced the asymmetric cosegregation of PKC λ /i and phospho-p38, seen as the increased percentage of SCs with asymmetric distribution of the two proteins in the same side of the cell (Fig. 3C, 3E).

Asymmetric localization of atypical PKC λ /i and phospho-p38 during SC division is closely related to the Par3-Par6-PKC λ /i complex ("Par complex") formation during SC asymmetric division [4]. The increased localization of both PKC λ /i and phospho-p38 observed in UnAG-treated SCs could depend on an enhanced Par complex formation. Therefore, we assessed if UnAG enhanced PKC λ /i and PAR3 complex formation within SCs using a PLA. We observed that indeed UnAG-treated SCs displayed an increased number of PLA dots compared to control (Fig. 3F, 3G), indicating that UnAG enhances Par complex assembly.

Asymmetric division depends on Par complex formation and its asymmetric localization [4] and, accordingly, incubation with 10 μ M aurothiomalate, an inhibitor of Par complex assembly [32], prevented the effect of UnAG on SC asymmetric division (Fig. 4A).

The activation of p38 in dividing SCs affects their ability to undergo self-renewal and, indeed, incubation of UnAG-

treated myofibers with 5 μ M of p38 inhibitor SB203580, completely abrogated UnAG effect on self-renewal (Fig. 4B). Altogether these data suggest that UnAG promotes SC asymmetric division and self-renewal through asymmetric phosphorylation of p38.

Incubation of UnAG-treated myofibers with 10 μ M NF449, a compound able to abolish the anti-atrophic activity of UnAG in C2C12 myotubes by uncoupling G α_s from G protein-coupled receptors (GPCRs) [14], abrogated the increment of atypical PKC/PAR3 complex induced by UnAG (Fig. 4C, 4D), supporting the hypothesis that UnAG acts through a G α_s -coupled GPCR, as previously suggested [14].

Upregulation of Circulating UnAG Protects Dystrophic Muscles Architecture and Functionality

The improved muscle regeneration in *Myh6/Ghrl* mice and enhanced SC activity within the muscle of *Myh6/Ghrl* mice and in response to UnAG treatment suggest that increase in UnAG may be beneficial for muscle diseases such as dystrophies, in which the lack of dystrophin impacts both on muscle fragility and on SC function, leading to chronic degeneration and impaired regeneration [18, 33]. To test the hypothesis that upregulation of UnAG circulating levels protects dystrophic muscles from deterioration, we crossed dystrophin-null mdx mice with hemizygous *Myh6/Ghrl* mice, producing mdx^{Tg+} mice and mdx^{Tg-} littermate controls. Histological analysis revealed that muscles of both animal groups were undergoing regeneration, seen as high density of Pax7⁺ SC and the presence of eMyHC⁺ fibers in diaphragms (Supporting Information Fig. 5A–5D). However, in mdx^{Tg+} mice compared to the mdx^{Tg-} littermates, displayed lower fiber damage in diaphragms of 1- and 3-month-old mice, while no differences were evident at 6 months of age (Fig. 5A, 5B). During the progression of the pathology, the gradual replacement of functional muscle with collagen in diaphragm was delayed in mdx^{Tg+} mice compared to the mdx^{Tg-} littermates, becoming significantly lower at 6 months of age (Fig. 5C, 5D), indicating that upregulation of UnAG ameliorates the dystrophic phenotype. Consistently, hanging-wire-test scores and latency-to-fall time, assessments of muscular functionality and endurance, were improved in mdx^{Tg+} mice starting from 4 months of age (Fig. 5E, 5F), showing that the differences highlighted by histological analysis translated into enhanced functional performance. Altogether, these data show that upregulation of circulating UnAG partially relieves the pathological condition of mdx dystrophic mice.

To assess if these UnAG activities could have clinical relevance, as a proof of concept, we exogenously administered UnAG to dystrophic mice using adeno-associated virus (AAV)-mediated delivery. We used the AAV9-*Ghrl* vector that has been demonstrated to protect the muscle from ischemic injury as the UnAG peptide does [11]. We injected 3.5×10^{11} vg of either AAV9-*Ghrl* or AAV9-*LacZ* in the tail vein of 3-week-old mdx mice, when the first round of muscle degeneration occurs [34], and analyzed the effect on muscles at 3 months of age. Ghrelin upregulation in muscles was confirmed by real-time RT-PCR (Supporting Information Fig. 6A, 6B). Analysis of diaphragms revealed less muscle damage (Fig. 5G, 5H) and collagen deposition (Fig. 5I, 5J) in AAV9-*Ghrl*-injected mice compared to the AAV9-*LacZ*-injected controls. Altogether, these data indicate that UnAG treatment is

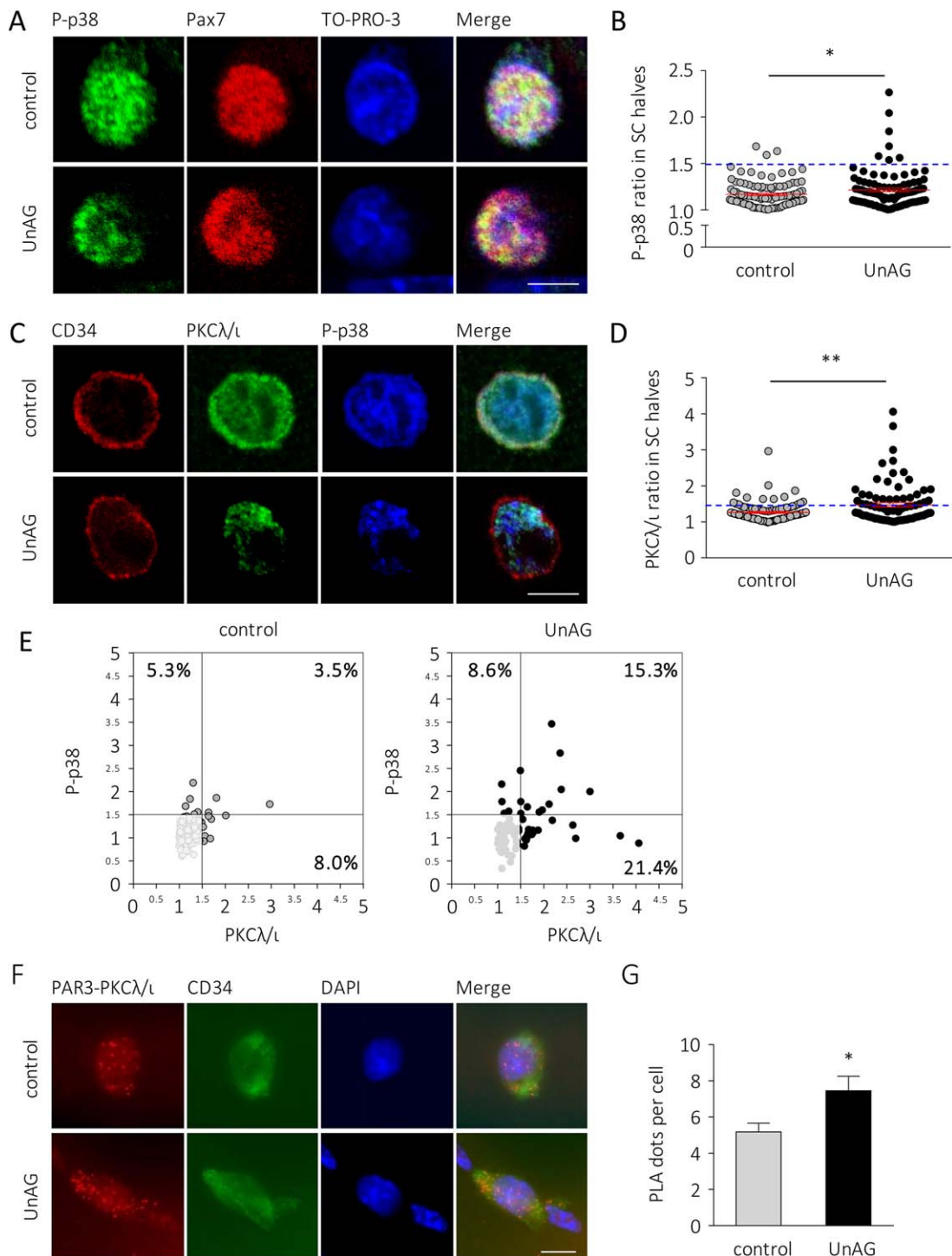


Figure 3. UnAG induces asymmetric localization of phospho-p38 and PKC λ/ι within the satellite cell and increases PAR3-PKC λ/ι complex formation. **(A):** Representative images and **(B)** quantification of asymmetric distribution of phospho-p38^{T180/Y182} in UnAG-treated versus untreated (control) SCs. Cells over the dashed line display at least 50% more phospho-p38^{T180/Y182} in one half of the nucleus compared to the other half. Mean \pm SEM *, $p < .05$; for each experiment ≥ 30 fibers/treatment, ≥ 34 SCs/treatment; $n = 3$ independent experiments. Scale bar, 5 μ m. **(C):** Representative images of PKC λ/ι and phospho-p38^{T180/Y182} distribution in control (top) and UnAG-treated (bottom) SCs (CD34+). Scale bar, 5 μ m. **(D):** Quantification of asymmetric distribution of PKC λ/ι in UnAG-treated versus untreated (control) SCs. Cells over the dashed line display at least 50% more PKC in one half of the nucleus compared to the other half. **, $p < .01$; for each experiment ≥ 30 fibers/treatment, ≥ 28 SCs/treatment; $n = 3$ independent experiments **(E):** Correlation between the asymmetric distribution of PKC λ/ι (x-axis) and phospho-p38^{T180/Y182} (y-axis) in control (left) versus UnAG-treated (right) SCs. Each dot denotes a single satellite cell. The bottom-left shadowed quadrants contain the SCs with both phospho-p38^{T180/Y182} and PKC λ/ι uniformly distributed. Total SCs counted $n = 202$ (control), 188 (UnAG-treated). **(F):** Representative images of the PLA-detected complexes of PAR3 and PKC λ/ι (red) in control (top) versus UnAG-treated (bottom) SCs (CD34+, green). Nuclei stained with DAPI. Scale bar, 5 μ m. **(G):** Quantification of the PLA dots per single satellite cell in control versus UnAG-treated SCs. Mean \pm SEM *, $p < .05$; for each experiment, ≥ 30 fibers, nuclei ≥ 69 (control), ≥ 70 (UnAG); $n = 3$ independent experiments. Abbreviations: DAPI, 4',6-diamidino-2-phenylindole; PLA, proximity ligation assay; SC, satellite cells; UnAG, unacylated ghrelin.

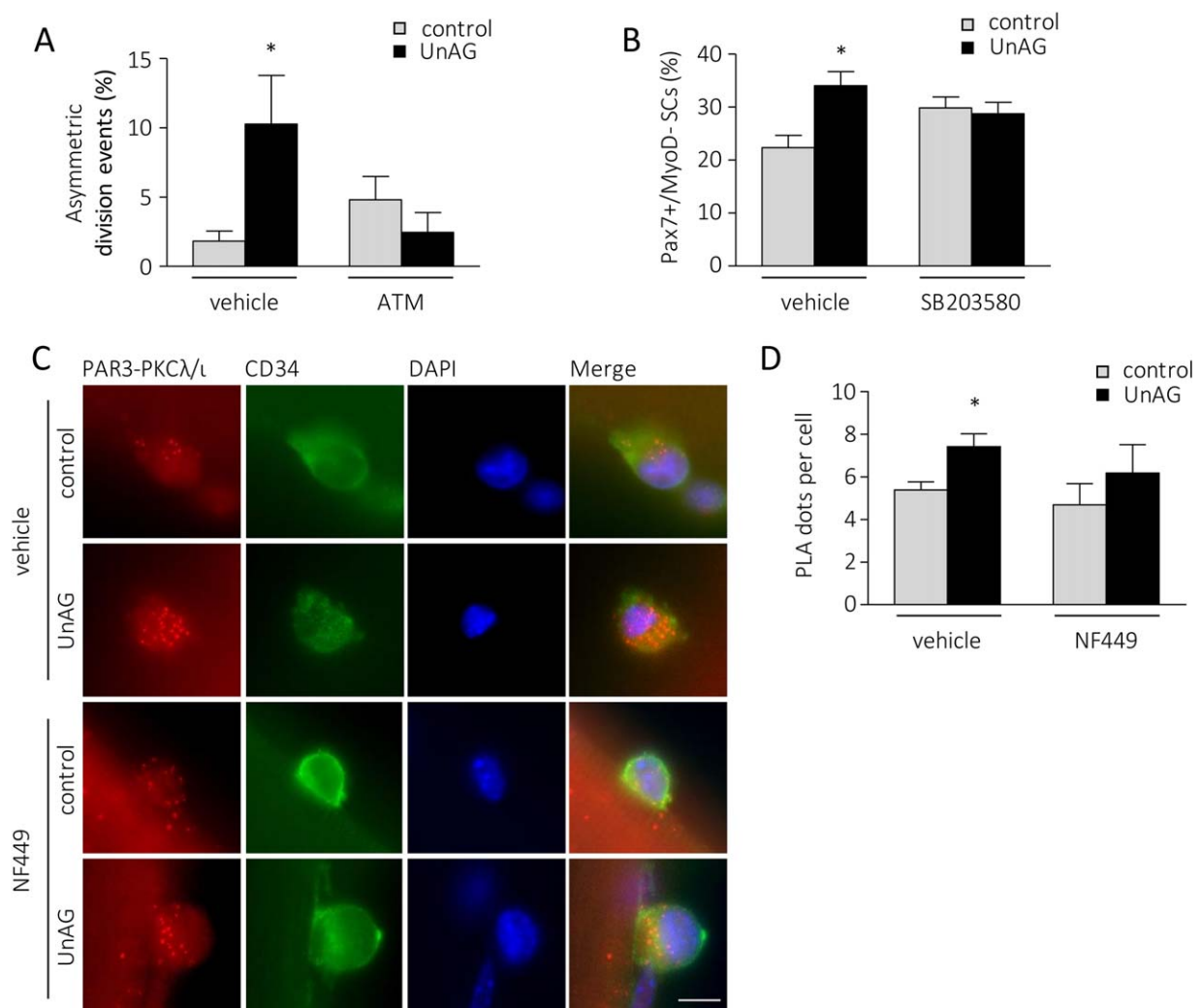


Figure 4. UnAG-induced satellite cell asymmetric division and self-renewal is mediated by Par complex assembly-p38 activation and occurs through a $G\alpha_s$ -coupled GPCR. **(A):** Percentage of asymmetric division events in SC doublets after 48 hours of UnAG treatment in the presence/absence of 10 μ M ATM, an inhibitor of atypical PKC λ /l-Par6 complex formation. Mean \pm SEM *, $p < .05$; ≥ 20 fibers/treatment, ≥ 22 doublets/treatment; $n = 4$ independent experiments. **(B):** Percentage of Pax7+/MyoD-SCs after 96 hours of UnAG treatment in the presence/absence of 5 μ M p38 inhibitor SB203580. Mean \pm SEM *, $p < .05$ versus DMSO-treated control; ≥ 25 myofibers/treatment, ≥ 50 clusters/treatment, ≥ 3 SCs/cluster; $n = 2$ independent experiments. **(C):** Representative images of PLA-detected complexes of PAR3 and PKC λ /l (red) in control versus UnAG-treated SCs (CD34+, green) in the presence or absence of 10 μ M NF499. Nuclei stained with DAPI. Scale bar, 5 μ m. **(D):** Quantification of the PLA dots per satellite cell. Mean \pm SEM *, $p < .05$; ≥ 30 fibers; n nuclei = 72 (control), 70 (UnAG), 81 (NF499), 45 (NF499 + UnAG); $n = 2$ independent experiments. Abbreviations: ATM, aurothiomalate; DAPI, 4',6-diamidino-2-phenylindole; PLA, proximity ligation assay; SC, satellite cells; UnAG, unacylated ghrelin.

effective even after the onset of muscle degeneration, supporting the idea that UnAG administration could represent a potential treatment for muscular dystrophies.

UnAG Enhances Dystrophin-Null Satellite Cell Self-Renewal and Myogenic Commitment

To assess the direct effect of UnAG on dystrophic SCs, we isolated EDL fibers from dystrophin-null mdx and WT mice, and we cultured them in the presence or absence of 100 nM UnAG for 96 hours. The number of Pax7+/MyoD- SCs was 60% lower in mdx fibers compared to the WT ones, indicating an intrinsic self-renewal defect of dystrophin-deficient SCs, in agreement with previously reported data [19]; however, UnAG significantly raised the Pax7+/MyoD- SC portion in both WT and mdx fibers (Fig. 6A, 6B). The relative increase of quiescent SCs, of about 50%, was the same in both WT and mdx fibers,

indicating that UnAG promotes SC self-renewal independently from the presence of dystrophin. Also, UnAG enhanced the number of myogenin-expressing SCs in mdx myofibers cultured for 72 hours (Fig. 6C, 6D), indicating that the increase of quiescent SCs does not imply an unbalance between self-renewal and myogenic commitment.

The sustained muscle regeneration in mdx mice is emphasized by the huge expansion of SCs that, however, in the long run, leads to the depletion of the SC pool. Although no significant differences in the number of SCs are evident in mdx^{Tg+} mice compared to mdx^{Tg-} muscles at 1- to 6-months-old animals (Supporting Information Fig. 5A, 5B), in diaphragms of 12-month-old mice we observed that the exhaustion of SC pool, characteristic of the advanced pathology [19], was less pronounced in mdx^{Tg+} mice compared to mdx^{Tg-} mice (Fig. 6E, 6F), coherently with the concept that UnAG promotes SC

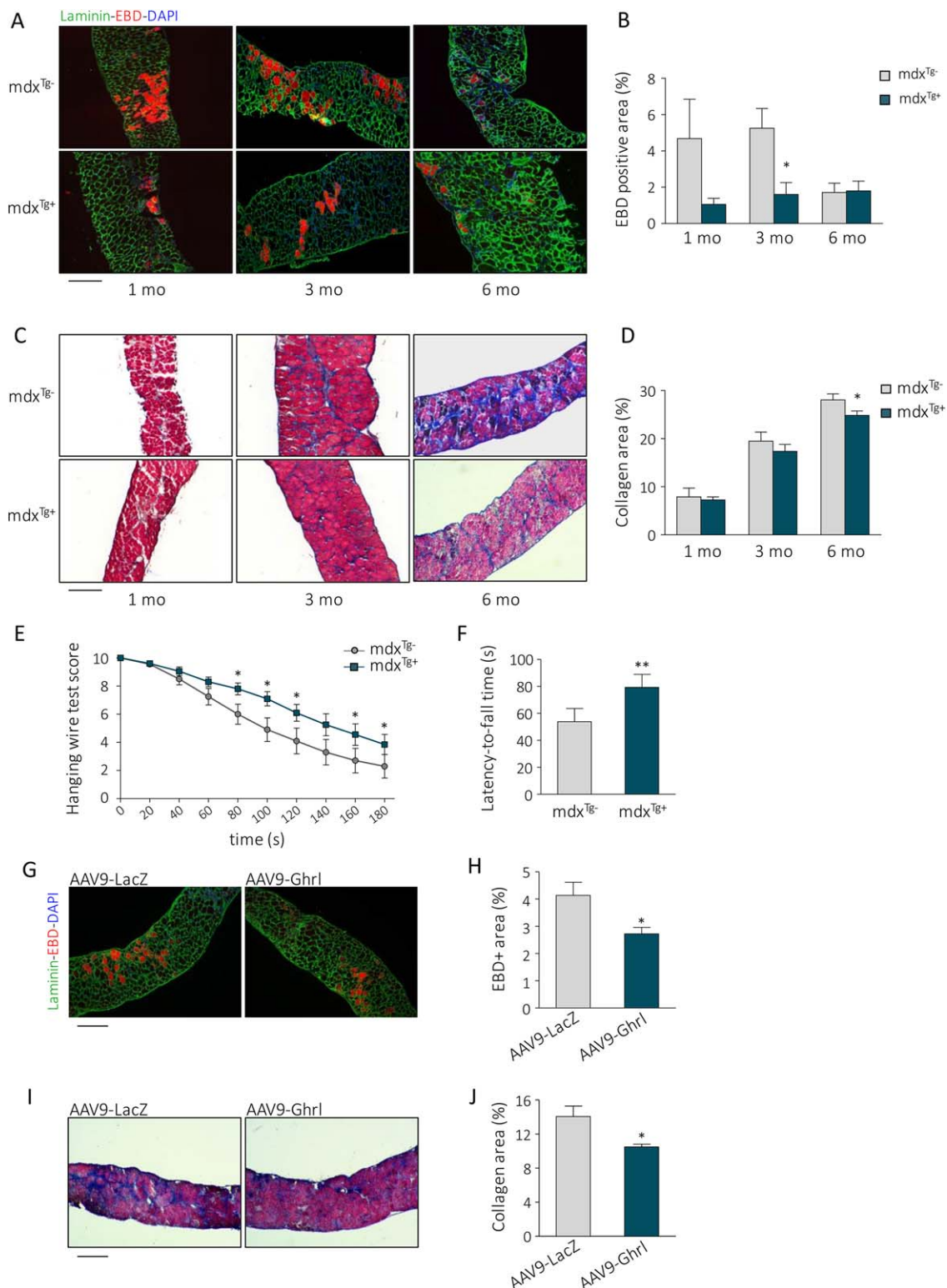


Figure 5. Unacylated ghrelin upregulation in mdx mice attenuates the dystrophic phenotype. **(A):** Representative images and **(B)** quantification of EBD uptake in diaphragms of 1- to 6-month-old mdx^{Tg-} and mdx^{Tg+} mice. Scale bar, 200 μ m. Mean \pm SEM **, $p < .01$ versus mdx^{Tg-}; $n = 7$ (mdx^{Tg-}) and 6 (mdx^{Tg+}). **(C):** Representative images of Masson trichrome staining and **(D)** quantification of collagen deposition in the diaphragm of 1- to 6-month-old mdx^{Tg+} and mdx^{Tg-} mice. Scale bar, 200 μ m. Mean \pm SEM *, $p < .05$; $n = 7$. **(E, F):** Muscular functionality measured by hanging wire test scores **(E)** and average latency-to-fall time **(F)** of 4-month-old mdx^{Tg-} and mdx^{Tg+} mice. Mean \pm SEM; *, $p < .05$ and **, $p < .01$ versus mdx^{Tg-}; $n = 20$. **(G):** Representative images and **(H)** quantification of Evan Blue Dye uptake in AAV9-LacZ- or AAV9-Ghrl-transduced diaphragms of 3-month-old mdx mice. Scale bar, 200 μ m. Mean \pm SEM *, $p < .05$ versus AAV9-LacZ-transduced muscles; $n = 5$. **(I):** Representative images and **(J)** quantification of collagen deposition in AAV9-LacZ- and AAV9-Ghrl-transduced diaphragms of 3-month-old mdx mice. Scale bar, 200 μ m. Mean \pm SEM *, $p < .05$ versus AAV9-LacZ-transduced muscles; $n = 5$. Abbreviations: DAPI, 4',6-diamidino-2-phenylindole; EBD, Evans blue dye.

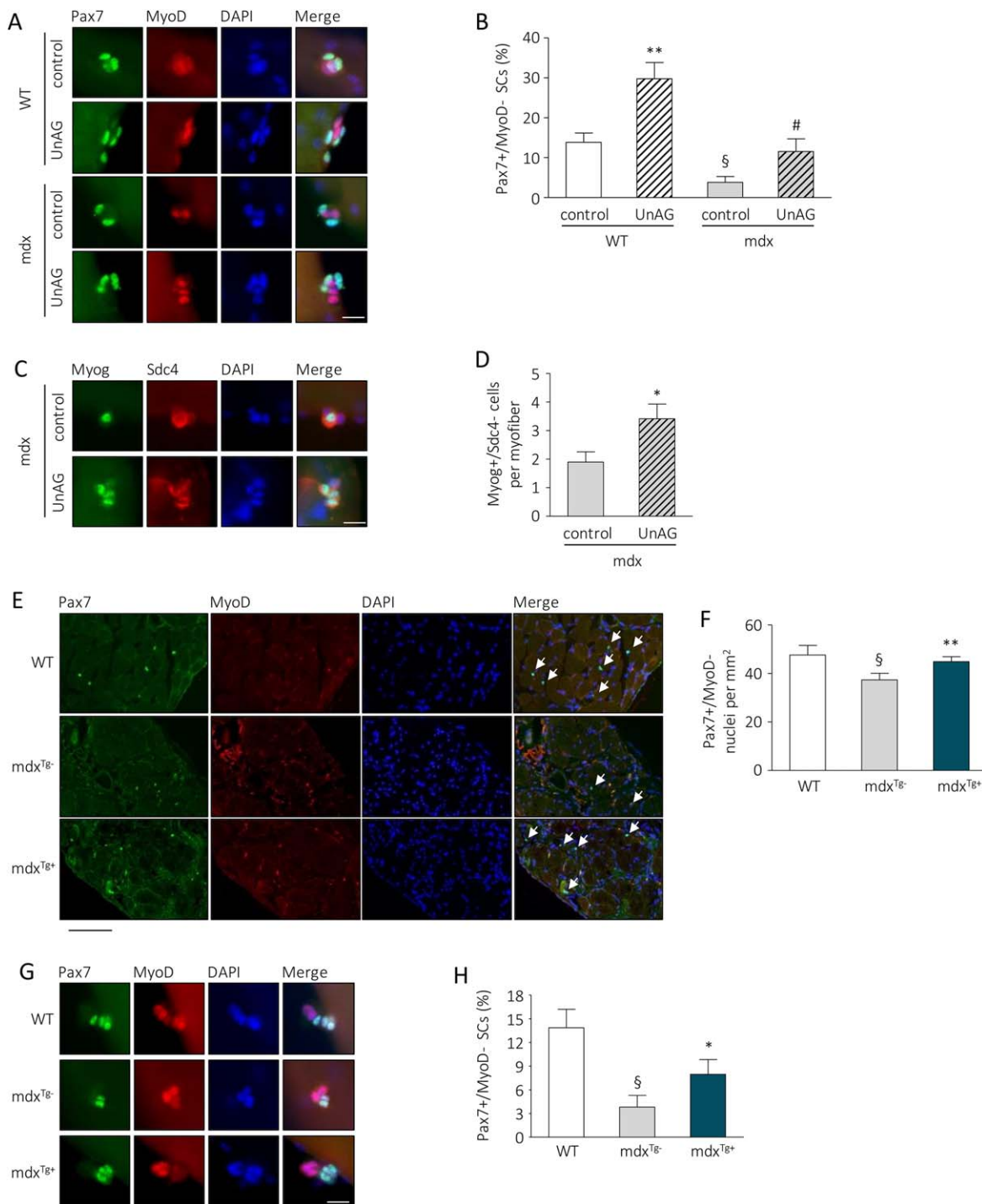


Figure 6. UnAG improves dystrophin-null SCs activity. **(A):** Representative images of Pax7 and MyoD IF and DAPI counterstaining of SCs on myofibers isolated from WT or mdx extensor digitorum longus (EDL) muscles and treated with 100 nM UnAG for 96 hours. Scale bars, 20 μ m. **(B):** Percentage of Pax7+/MyoD- SCs after 96 hours of treatment of WT or mdx myofibers with 100 nM UnAG. Mean \pm SEM. **, $p < .01$ versus WT control, §, $p < .01$ versus WT control, and #, $p < .01$ versus mdx control. ≥ 25 myofibers/treatment, ≥ 14 cluster/treatment, ≥ 3 SCs/cluster; single experiment. **(C):** Representative images of Myog and Sdc4 IF and DAPI counterstaining of SCs on myofibers isolated from mdx EDL muscles and treated with 100 nM UnAG for 72 hours. Scale bar, 20 μ m. **(D):** Number of Myog+/Sdc4- SCs per fibers after 72 hours of treatment of mdx myofibers with 100 nM UnAG. *, $p < .01$ versus mdx, ≥ 45 myofibers/treatment, total Myog+/Sdc4- SCs = 95 (control), 140 (UnAG); $n = 3$ independent experiments. **(E):** Representative images (scale bar, 200 μ m) and **(F)** quantification of Pax7+/MyoD- (arrows) cells/mm² in diaphragm sections of 12-month-old mdx^{Tg+} and mdx^{Tg-} mice. Mean \pm SEM §, $p < .05$ versus WT; *, $p < .05$ versus mdx^{Tg-}; $n = 7$. **(G):** Representative images (scale bar, 20 μ m) and **(H)** percentage of Pax7+/MyoD- SCs on myofibers isolated from aged (12 months) WT, mdx^{Tg-}, and mdx^{Tg+} cultured for 96 hours in low proliferation medium. §, $p < .01$ versus WT control and *, $p < .05$ versus mdx^{Tg-}, ≥ 23 myofibers/group, ≥ 23 cluster/group, ≥ 3 SCs/cluster; single experiment. Abbreviations: DAPI, 4',6-diamidino-2-phenylindole; Myog, myogenin; SCs, satellite cells; Sdc4, syndecan 4; UnAG, unacylated ghrelin; WT, wild type mice.

self-renewal. Consistently, after 96 hours in culture, myofibers from mdx^{Tg+} mice displayed twice as much Pax7+/MyoD-SCs, likely reflecting an initial higher content of functional SCs (i.e., able to undergo self-renewal) compared to mdx^{Tg-} mice (Fig. 6G, 6H).

DISCUSSION

The data herein presented demonstrate that UnAG acts on SCs enhancing their activation, differentiation, and self-renewal. SC self-renewal depends on either symmetric or asymmetric division of a subpopulation of noncommitted progenitors. For instance, Wnt7a promotes SC self-renewal through induction of their symmetric division via a noncanonical, planar-cell-polarity pathway [35] and without affecting SC differentiation. On the contrary, UnAG promotes SC self-renewal enhancing at the same time their terminal differentiation, as shown by the increase of fusion index on cultured SCs (Supporting Information Fig. 7). This effect is likely a consequence of UnAG-induced increase on SC asymmetric division that simultaneously maintains the stem compartment of MyoD- SCs and expands the number of the committed MyoD+ myoblasts able to respond to the pro-differentiative activity of UnAG, in agreement with the effect observed on C2C12 [16].

SC asymmetric division is sustained by the Par polarity complex that includes the atypical PKC λ /i, which controls the asymmetric activation of p38 that, in turn, triggers MyoD expression and myogenic commitment in only one daughter cell [4, 5]. Phosphorylated p38 plays a key role in asymmetric division [4]; indeed, loss or reduction of asymmetric segregation of phosphorylated p38 and its diffuse activation within the SC from aged mice determines a strong decline of asymmetric division events and the consequent impairment of SC self-renewal ability [28].

UnAG promotes the asymmetric cosegregation of PKC λ /i and phospho-p38 and the Par complex assembly in myofiber-associated SCs. In addition, uncoupling of PKC λ /i from the Par complex and inhibition of p38 activity impair UnAG-induced asymmetric division and self-renewal, indicating that UnAG triggers signaling pathways contributing to the formation of the polarity complex. The finding that uncoupling of G α_s from GPCRs impairs the UnAG-stimulated assembly of the polarity complex suggests that UnAG acts in SCs through a similar or the same receptor mediating its anti-atrophic activity in C2C12 myotubes [14]. The lack of knowledge on the identity of UnAG receptor hinders deeper investigations on the signaling mechanisms mediating its activity in SCs. Nevertheless, UnAG stimulates cAMP and PKA [36], which are linked to the activation of the polarity kinase LKB1 and to the formation of the polarity complex [37–39], thus leading to the speculation that cAMP/PKA pathway may contribute to UnAG polarizing signal in SCs.

The expansion of SCs through asymmetric division and the enhancement of their differentiation elicited by UnAG underline its ability to enhance skeletal muscle regeneration (Fig. 1A–1C, [10, 11]), consistently with the hypothesis that ghrelin induction in the injured muscle contributes to the repair process. Indeed, ghrelin is rapidly and transiently induced upon muscle damage [24]. However, the identification of the cells responsible for ghrelin expression is hampered by the poor specificity of the

available anti-preproghrelin antibodies, which recognize positive signals in injured skeletal muscle of ghrelin KO mice (data not shown). As ghrelin is highly expressed in neutrophils, which are recruited to the site of damage with similar kinetics as ghrelin induction [40, 41], we can speculate that neutrophils may be responsible for ghrelin upregulation observed in muscles after injury. Altogether these findings suggest that UnAG is part of the damage-induced tissue repair process.

The more efficient engraftment of donor SCs in Tg mice (Fig. 1F, 1G) is consistent with a direct effect on SC functionality as well. However, the better engraftment may also depend on UnAG anti-inflammatory activity. Indeed, in skeletal muscle, UnAG inhibits TNF- α expression following either burn injury or high-fat diet [12, 15]. Furthermore, we cannot rule out that the increased engraftment of SCs in Tg muscle may partially be due to an anti-apoptotic effect of UnAG on transplanted SCs since UnAG inhibits apoptosis in both cardiomyocytes and myoblasts through activation of autophagy [11, 12].

Altogether, these findings indicate that UnAG regulates multiple steps of muscle regeneration by stimulating asymmetric division-mediated SC self-renewal and by promoting terminal differentiation and fusion of proliferating myoblasts. The capacity of UnAG to induce SC self-renewal also in vivo translates in the ability to preserve the quiescent SC pool upon repeated cycles of injury/regeneration.

UnAG pro-regenerative effect on skeletal muscle and its activity on SCs may account for the less severe phenotype observed in dystrophic mice with high levels of circulating or local UnAG in mdx^{Tg+} or AAV-Ghrl-treated mdx mice, respectively. However, the anti-inflammatory, and, consequently, the anti-fibrotic activities of UnAG [42, 43] could be likewise relevant to explain the protection of tissue architecture and the amelioration of muscle performance. In addition, as defective basal autophagy contributes to the dystrophic phenotype [44, 45], UnAG-enhanced autophagy may likewise contribute to its protective activity in mdx mice.

In dystrophy, the exhaustion of the SC pool has been assumed to cause the failure of regeneration to keep up with muscle damage. However, in both human and mice SC pool exhaustion likely sets in only at late stages of the pathology as a consequence of defective SC self-renewal [19]. Furthermore, dystrophic muscles show an increased overall number of SCs, although, within this figure, the portion of quiescent SCs is reduced, reflecting an ongoing regeneration [18, 19, 46]. It is plausible that the defect in muscle regeneration of mdx mice resides at least in part in the defective asymmetric division of dystrophin-null SC that translates in an imbalance between SCs and committed myoblasts able to terminally differentiate and repair the damaged muscle [18, 33]. The finding that UnAG, in dystrophin-null SCs, enhances their self-renewal and increases the number of committed myoblasts suggests that UnAG promotes SC asymmetric division by activating pathways that are independent of dystrophin expression. Thus, we can speculate that the increase in the absolute number of functional SCs triggered by UnAG in mdx mice may increase the number of committed progenitors, thus sustaining the better muscle regeneration and improved dystrophic phenotype observed in mdx^{Tg+} mice.

Altogether, these data suggest that increase in either circulating or local UnAG levels could delay the progression of the disease. A therapeutic approach would presumably involve the chronic administration of UnAG to dystrophic patients.

Although the receptor through which UnAG exerts its biological activities remains elusive, UnAG has been recently used in clinical trials to assess its metabolic effects, and it was reported that the peptide was well tolerated, and no serious adverse events occurred during the studies [47–51]; therefore, UnAG could be a realistic adjuvant treatment in the near future to help to preserve muscles of dystrophic patients.

SUMMARY

UnAG affects in multiple ways SC physiological behavior and enhances skeletal muscle regeneration. These activities result in an overall beneficial effect in dystrophic mdx mice, seen as an improved condition of muscles and a better physical performance, and suggest that UnAG could be regarded as a realistic therapeutic strategy for muscular dystrophies, either as a self-sufficient treatment or as an adjuvant with other therapies.

ACKNOWLEDGMENTS

This study was supported by research grants from the Muscular Dystrophy Association (Grant MDA294617 to N.F. and A.G.),

AFM-Téléthon (Grant 16437 to A.G.) and Compagnia di San Paolo (to A.G. and N.F.). E.A., M.F., V.M., S.C., and A.G. are currently affiliated with the Università Vita-Salute San Raffaele, Milano, Italy.

AUTHOR CONTRIBUTIONS

S.R., E.A., and M.F.: conception and design; collection and/or assembly of data; data analysis and interpretation; manuscript writing; V.M. and H.S.: conception and design; collection and/or assembly of data; data analysis and interpretation; final approval of manuscript; O.S., E.A., S.C., and G.R.: collection and/or assembly of data; final approval of manuscript; L.Z. and S.G.: provision of study material; final approval of manuscript; F.P.: data analysis and interpretation; final approval of manuscript; M.G.: conception and design; final approval of manuscript; A.G. and N.F.: conception and design; data analysis and interpretation; manuscript writing.

DISCLOSURE OF POTENTIAL CONFLICTS OF INTEREST

The authors indicated no potential conflicts of interest.

REFERENCES

- Seale P, Sabourin LA, Girgis-Gabardo A et al. Pax7 is required for the specification of myogenic satellite cells. *Cell* 2000;102:777–786.
- Collins CA, Olsen I, Zammit PS et al. Stem cell function, self-renewal, and behavioral heterogeneity of cells from the adult muscle satellite cell niche. *Cell* 2005;122:289–301.
- Kuang S, Kuroda K, Le Grand F et al. Asymmetric self-renewal and commitment of satellite stem cells in muscle. *Cell* 2007;129:999–1010.
- Troy A, Cadwallader AB, Fedorov Y et al. Coordination of satellite cell activation and self-renewal by Par-complex-dependent asymmetric activation of p38 α / β MAPK. *Cell Stem Cell* 2012;11:541–553.
- Jones NC, Tyner KJ, Nibarger L et al. The p38 α /beta MAPK functions as a molecular switch to activate the quiescent satellite cell. *J Cell Biol* 2005;169:105–116.
- Gutierrez JA, Solenberger PJ, Perkins DR et al. Ghrelin octanoylation mediated by an orphan lipid transferase. *Proc Natl Acad Sci USA* 2008;105:6320–6325.
- Yang J, Brown MS, Liang G et al. Identification of the acyltransferase that octanoylates ghrelin, an appetite-stimulating peptide hormone. *Cell* 2008;132:387–396.
- Kojima M, Hosoda H, Date Y et al. Ghrelin is a growth-hormone-releasing acylated peptide from stomach. *Nature* 1999;402:656–660.
- Müller TD, Nogueiras R, Andermann ML et al. Ghrelin. *Mol Metab* 2015;4:437–460.
- Togliatto G, Trombetta A, Dentelli P et al. Unacylated ghrelin promotes skeletal muscle regeneration following hindlimb ischemia via SOD-2-mediated miR-221/222 expression. *J Am Heart Assoc* 2013;2:e000376.
- Ruozi G, Bortolotti F, Falcione A et al. AAV-mediated in vivo functional selection of tissue-protective factors against ischaemia. *Nat Commun* 2015;6:7388.
- Gortan Cappellari G, Zanetti M, Semolic A et al. Unacylated ghrelin reduces skeletal muscle reactive oxygen species generation and inflammation and prevents high-fat diet induced hyperglycemia and whole-body insulin resistance in rodents. *Diabetes* 2016;65:874–886.
- Tam BT, Pei XM, Yung BY et al. Unacylated ghrelin restores insulin and autophagic signaling in skeletal muscle of diabetic mice. *Pflügers Arch* 2015;467:2555–2569.
- Porporato PE, Filigheddu N, Reano S et al. Acylated and unacylated ghrelin impair skeletal muscle atrophy in mice. *J Clin Invest* 2013;123:611–622.
- Sheriff S, Kadeer N, Joshi R et al. Des-acyl ghrelin exhibits pro-anabolic and anti-catabolic effects on C2C12 myotubes exposed to cytokines and reduces burn-induced muscle proteolysis in rats. *Mol Cell Endocrinol* 2012;351:286–295.
- Filigheddu N, Gnocchi VF, Coscia M et al. Ghrelin and des-acyl ghrelin promote differentiation and fusion of C2C12 skeletal muscle cells. *Mol Biol* 2007;18:986–994.
- Wallace GQ, McNally EM. Mechanisms of muscle degeneration, regeneration, and repair in the muscular dystrophies. *Annu Rev Physiol* 2009;71:37–57.
- Dumont NA, Wang YX, von Maltzahn J et al. Dystrophin expression in muscle stem cells regulates their polarity and asymmetric division. *Nat Med* 2015;21:1455–1463.
- Jiang C, Wen Y, Kuroda K et al. Notch signaling deficiency underlies age-dependent depletion of satellite cells in muscular dystrophy. *Dis Model Mech* 2014;7:997–1004.
- Raymackers JM, Debaix H, Colson-Van Schoor M et al. Consequence of parvalbumin deficiency in the mdx mouse: Histological, biochemical and mechanical phenotype of a new double mutant. *Neuromuscul Disord* 2003;13:376–387.
- van Putten M, de Winter C, van Roon-Mom W et al. A 3 months mild functional test regime does not affect disease parameters in young mdx mice. *Neuromuscul Disord* 2010;20:273–280.
- Yablonka-Reuveni Z, Rivera AJ. Temporal expression of regulatory and structural muscle proteins during myogenesis of satellite cells on isolated adult rat fibers. *Dev Biol* 1994;164:588–603.
- Crist CG, Montarras D, Buckingham M. Muscle satellite cells are primed for myogenesis but maintain quiescence with sequestration of Myf5 mRNA targeted by microRNA-31 in mRNP granules. *Cell Stem Cell* 2012;11:118–126.
- Gurriarán-Rodríguez U, Santos-Zas I, Al-Massadi O et al. The obestatin/GPR39 system is up-regulated by muscle injury and functions as an autocrine regenerative system. *J Biol Chem* 2012;287:38379–38389.
- Bischoff R. Regeneration of single skeletal muscle fibers in vitro. *Anat Rec* 1975;182:215–235.
- Olguin HC, Olwin BB. Pax-7 up-regulation inhibits myogenesis and cell cycle progression in satellite cells: A potential mechanism for self-renewal. *Dev Biol* 2004;275:375–388.
- Zammit PS, Golding JP, Nagata Y et al. Muscle satellite cells adopt divergent fates: A mechanism for self-renewal?. *J Cell Biol* 2004;166:347–357.
- Bernet JD, Doles JD, Hall JK et al. p38 MAPK signaling underlies a cell-autonomous loss of stem cell self-renewal in skeletal muscle of aged mice. *Nat Med* 2014;20:265–271.
- Shea KL, Xiang W, LaPorta VS et al. Sprouty1 regulates reversible quiescence of a self-renewing adult muscle stem cell pool during regeneration. *Cell Stem Cell* 2010;6:117–129.

- 30** Buono R, Vantaggiato C, Pisa V et al. Nitric oxide sustains long-term skeletal muscle regeneration by regulating fate of satellite cells via signaling pathways requiring Vangl2 and cyclic GMP. *STEM CELLS* 2012;30:197–209.
- 31** Palacios D, Puri PL. The epigenetic network regulating muscle development and regeneration. *J Cell Physiol* 2006;207:1–11.
- 32** Stallings-Mann M, Jamieson L, Regala RP et al. A novel small-molecule inhibitor of protein kinase C α blocks transformed growth of non-small-cell lung cancer cells. *Cancer* 2006;66:1767–1774.
- 33** Chang NC, Chevalier FP, Rudnicki MA. Satellite cells in muscular dystrophy – lost in polarity. *Trends Mol Med* 2016;22:479–496.
- 34** Grounds MD, Radley HG, Lynch GS et al. Towards developing standard operating procedures for pre-clinical testing in the mdx mouse model of Duchenne muscular dystrophy. *Neurobiol Dis* 2008;31:1–19.
- 35** Le Grand F, Jones AE, Seale V et al. Wnt7a activates the planar cell polarity pathway to drive the symmetric expansion of satellite stem cells. *Cell Stem Cell* 2009;4:535–547.
- 36** Granata R, Settanni F, Biancone L et al. Acylated and unacylated ghrelin promote proliferation and inhibit apoptosis of pancreatic beta-cells and human islets: Involvement of 3',5'-cyclic adenosine monophosphate/protein kinase A, extracellular signal-regulated kinase 1/2, and phosphatidylinositol. *Endocrinology* 2007;148:512–529.
- 37** Collins SP, Reoma JL, Gamm DM et al. LKB1, a novel serine/threonine protein kinase and potential tumour suppressor, is phosphorylated by cAMP-dependent protein kinase (PKA) and prenylated in vivo. *Biochem J* 2000;345:673–680.
- 38** Bernard LP, Zhang H. MARK/Par1 kinase is activated downstream of NMDA receptors through a PKA-dependent mechanism. *PLoS One* 2015;10:1–11.
- 39** Shen YA, Chen Y, Dao DQ et al. Phosphorylation of LKB1/Par-4 establishes Schwann cell polarity to initiate and control myelin extent. *Nat Commun* 2014;5:4991.
- 40** Hattori N, Saito T, Yagyu T et al. GH, GH receptor, GH secretagogue receptor, and Ghrelin expression in human T cells, B cells, and neutrophils. *J Clin Endocrinol Metab* 2001;86:4284–4291.
- 41** Tidball JG, Villalta SA. Regulatory interactions between muscle and the immune system during muscle regeneration. *Am J Physiol Regul Integr Comp Physiol* 2010;298:R1173–R1187.
- 42** Prodam F, Filigheddu N. Ghrelin gene products in acute and chronic inflammation. *Arch Immunol Ther Exp (Warsz)* 2014;62:369–384.
- 43** Angelino E, Reano S, Ferrara M et al. Anti-fibrotic activity of acylated and unacylated ghrelin. *Int J Endocrinol* 2015;2015:38568.
- 44** De Palma C, Morisi F, Cheli S et al. Autophagy as a new therapeutic target in Duchenne muscular dystrophy. *Cell Death Dis* 2012;3:e418.
- 45** Pal R, Palmieri M, Loehr JA et al. Src-dependent impairment of autophagy by oxidative stress in a mouse model of Duchenne muscular dystrophy. *Nat Commun* 2014;5:4425.
- 46** Kottlors M, Kirschner J. Elevated satellite cell number in Duchenne muscular dystrophy. *Cell Tissue Res* 2010;340:541–548.
- 47** Broglio F, Gottero C, Prodam F et al. Non-acylated ghrelin counteracts the metabolic but not the neuroendocrine response to acylated ghrelin in humans. *J Clin Endocrinol Metab* 2004;89:3062–3065.
- 48** Kiewiet RM, Van Aken MO, Van Der Weerd K et al. Effects of acute administration of acylated and unacylated ghrelin on glucose and insulin concentrations in morbidly obese subjects without overt diabetes. *Eur J Endocrinol* 2009;161:567–573.
- 49** Benso A, St-Pierre DH, Prodam F et al. Metabolic effects of overnight continuous infusion of unacylated ghrelin in humans. *Eur J Endocrinol* 2012;166:911–916.
- 50** Özcan B, Neggers SJM, Miller AR et al. Does des-acyl ghrelin improve glycemic control in obese diabetic subjects by decreasing acylated ghrelin levels? *Eur J Endocrinol* 2014;170:799–807.
- 51** Tong J, Davis HW, Summer S et al. Acute administration of unacylated ghrelin has no effect on basal or stimulated insulin secretion in healthy humans. *Diabetes* 2014;63:2309–2319.



See www.StemCells.com for supporting information available online.